INNSPUB

International Journal of Biosciences | IJB |
ISSN: 2220-6655 (Print), 2222-5234 (Online)
http://www.innspub.net
Vol. 13, No. 6, p. 176-185, 2018

RESEARCH PAPER OPEN ACCESS

Characterization of Fe_3O_4 nanoparticles for liquid phase immunoassay using brownian relaxation time and magnetic susceptibility

Md. Anwarul Kabir Bhuiya[1*], Raihana Ferdaws[1], Md. Abdul Halim[1], Takeshi YOSHIDA[2], Keiji Enpuku[2], Edmund Soji Otabe[3]

[1]*Department of Materials Science and Engineering, University of Rajshahi, Rajshahi, Bangladesh*

[2]*Department of Electrical and Electronic Engineering, Kyushu University, Fukuoka 819-0395, Japan*

[3]*Computer Science and Electronics, Kyushu Insitute of Technology, Iizuka, Japan*

Key words: Magnetic marker, Brownian relaxation, AC susceptibility, Magnetic moment, Size distribution, Singular value decomposition (SVD), Biosensor.

http://dx.doi.org/10.12692/ijb/13.6.176-185 Article published on December 23, 2018

Abstract

This article describes the detail characterization of the magnetic properties of magnetic markers (Fe_3O_4) in solution for biosensor application. Frequency dependence of the AC susceptibility and the magnetization curve, which were dominated by the Brownian rotation of the marker, Brownian relaxation time were measured. The effect of the viscosity of the carrier liquid on the AC susceptibility was also clarified. The experimental results were analyzed by the singular value decomposition (SVD) method. The distribution of marker size d was obtained from the frequency dependence of the AC susceptibility. The distribution of magnetic moment m was obtained from the magnetization curve. The relationship between m and d was also discussed. The present estimation method using SVD technique will be useful to obtain the distribution of particle size d and magnetic moment m, which are the important parameters of the magnetic marker for biomedical application. We also obtained the distributions of magnetic moment m and anisotropy energy barrier E_B, and their relationship. From the obtained result, we could classify the particles into three types: Type-I particles with very small m and very short τ_N, Type-II particles with medium values of m and τ_N, and Type-III particles with large m and very long τ_N.

* **Corresponding Author:** Md. Anwarul Kabir Bhuiya ✉ mkabir@ru.ac.bd

Introduction

Magnetic markers, which are composed of polymer-coated magnetic nanoparticles, have been extensively studied for use in biological applications such as cell separation, immunoassays, hyperthermia, and drug delivery. Immunoassays are used to detect biological targets such as disease-related proteins and cells. Magnetic immunoassay techniques that utilize magnetic markers have recently been developed. One of the advantages of this magnetic method is that we can perform immunoassays in the liquid phase; that is, we can magnetically distinguish bound markers from unbound (free) markers. This function can be utilized to eliminate the time-consuming washing process used to separate the two types of markers, i.e., the so-called bound/free separation [1, 2, 3].

This function can be realized by utilizing the Brownian relaxation of magnetic markers in the solution. The difference in the Brownian relaxation time between the bound and free markers can be exploited for the use in liquid-phase immunoassays. For this purpose, several methods have been proposed to prolong the relaxation time of the bound markers. The resulting difference between the magnetic properties of the bound and free markers has been detected using relaxation or susceptibility measurement. [4, 5, 6].

When we apply the Brownian relaxation method for the liquid phase immunoassay, the hydrodynamic diameter d_h, magnetic moment m_B, and anisotropy energy E_B are the key parameters of a magnetic marker because they determine the performance of the magnetic immunoassay. The hydrodynamic diameter d_h determines the Brownian relaxation timeτ_B, and the magnetic moment m_B determines the signal detected from the markers. The anisotropy energy E_B determines the Neel relaxation timeτ_N, which must be much longer than τ_B. Therefore, it is necessary to quantitatively evaluate these parameters for practical markers.[18] However, it must be noted that practical markers are usually composed of aggregated magnetic particles. As a result, their magnetic behavior will be different from those expected from single-domain nanoparticles. These points have not yet been clarified quantitatively. [4, 11, 17].

Experimental results

Experimental setup and sample

In this experiment, we used commercial magnetic markers supplied from Ocean Nanotech Company, USA. The marker composed of polymer coated Fe_3O_4 particles, whose specific diameter was 50 nm, and was dispersed in solution with concentration of 5 mg/ml. The 2 μl of the marker solution was diluted by 73 μl of the solution that consisted of the mixture of water and glycerol.

The concentration of the glycerol was changed from 0% to 75% in order to change the viscosity of the solution. In Figure1, an experimental setup is schematically shown. The excitation field of $H = H_a \sin 2\pi ft$ was applied by an excitation coil. A disk-shaped sample plate which contained 60 μl of the marker solution in its well was used. The size of the well was 5 mm in diameter. The sample plate was rotated by an ultrasonic motor and was positioned under the excitation coil. In this case, the markers were magnetized and had a magnetic moment m. The signal field Bs generated by m was detected by a magneto-resistive (MR) sensor (Honeywell, USA) that was installed 2 mm under the sample plate. The output signal of the MR sensor was connected to the lock-in amplifier in order to obtain both the real and imaginary parts of the signal. [19, 20].

AC susceptibility

Frequency dependences

Measurements of the frequency dependence of the AC susceptibility are shown in Figure 2. The real part χ' and the imaginary part χ'' are shown in Figurers. 2(a) and 2(b), respectively. As shown, the real part χ' decreased monotonically with frequency. On the other hand, the imaginary part χ'' had a peak value at some frequency: we define the frequency, which gives the maximum value of χ'' by f_p. It is well known that this peak frequency is related to the Brownian relaxation time τ_B of the marker as$f_p = 1/(2\pi\tau_B)$.

Table 1. Samples with different concentration of glycerol. Viscosity of the mixed solution was normalized by that of pure water (sample 1).

Sample	1	2	3	4	5	6
Water (%)	100	85	70	55	40	25
Glycerol (%)	0	15	30	45	60	75
f_p (Hz)	2500	1750	1000	390	120	70
Viscosity	1	1.4	2.5	6.4	21	36

The peak frequencies f_p significantly changed among samples. They were approximately 2500, 1750, 1000, 390, 120 and 70 Hz for the samples 1 to 6, respectively. This large change of f_p was due to the difference in the viscosity of the carrier liquid, as will be shown below. [19, 21].

Effect of different viscosity liquid

As shown in Figure 2 (b), the peak frequency became lower from sample 1 to 6. As listed in Table 1, this corresponds to the increase of the glycerol concentration in the solution. Since the viscosity of the glycerol is much higher than that of the water, the viscosity of the mixed solution becomes higher with the increase of the glycerol concentration. The effective viscosity of the mixed solution can be obtained as follows.

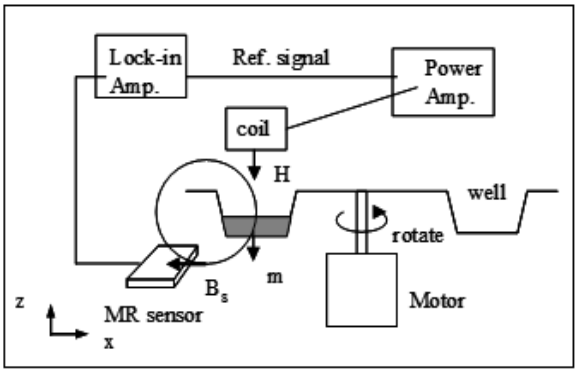

Fig. 1. Block diagram of the experimental set up.

It is well known that the Brownian relaxation time is given by $\tau_B = 3\eta V_h/k_BT$, where η is the viscosity of the liquid; V_h is the hydrodynamic volume of the particle. Therefore, the peak frequency f_p is inversely proportional to the viscosity η. using the measured value of f_p listed in Table 1, we can estimate the viscosity of each sample. In Figure 3, viscosity of samples, which was normalized by that of pure water (sample 1), was shown as a function of the concentration ratio of glycerol. As shown, viscosity of the mixed solution became 1.4, 2.5, 6.4, 21 and 36 times larger than that of water (sample 1) for samples 2 to 6. [21].

Analysis

Expression for susceptibility and magnetization

We analyze the experimental results shown in this section by taking account of the distribution of size d and magnetic moment m of the marker. In this case, we define the parameters as follow. The diameter of the $i-th$ magnetic nanoparticle is d_{mi}, thickness of the coating material is t, and the hydrodynamic diameter of the marker is $d_{hi} = d_{mi} + 2t$. Distribution function of the diameter is $f(d_h)$. then, the number of $i-th$ markers is $n_i = f_i(d_{hi})\Delta d_{hi}$, and the magnetic moment is given by $m_i = \mu_0 M_s V_{mi}$ where $V_{mi} = (\pi/6)d_{mi}^3$ is the volume of the magnetic nanoparticle and M_s is the saturation magnetization.

When a small AC field is applied, the real and imaginary parts of the susceptibility are given by [12, 13],

$$\chi'(\omega) = \frac{1}{3\mu_0 k_B T V_T}\sum_i \frac{n_i m_i^2}{1+(\omega\tau_i)^2} + \chi_\infty \quad (1)$$

$$\chi''(\omega) = \frac{1}{3\mu_0 k_B T V_T}\sum_i \frac{\omega\tau_i n_i m_i^2}{1+(\omega\tau_i)^2} \quad (2)$$

where k_B is the Boltzmann constant, $V_T = \sum n_i {m_i}^2$ is the total volume of the sample, and χ_∞ represents the susceptibility at high frequency limit. The relaxation time of the Brownian rotation of the particle is given by $\tau_i = \frac{3\eta V_{hi}}{k_B T}$.

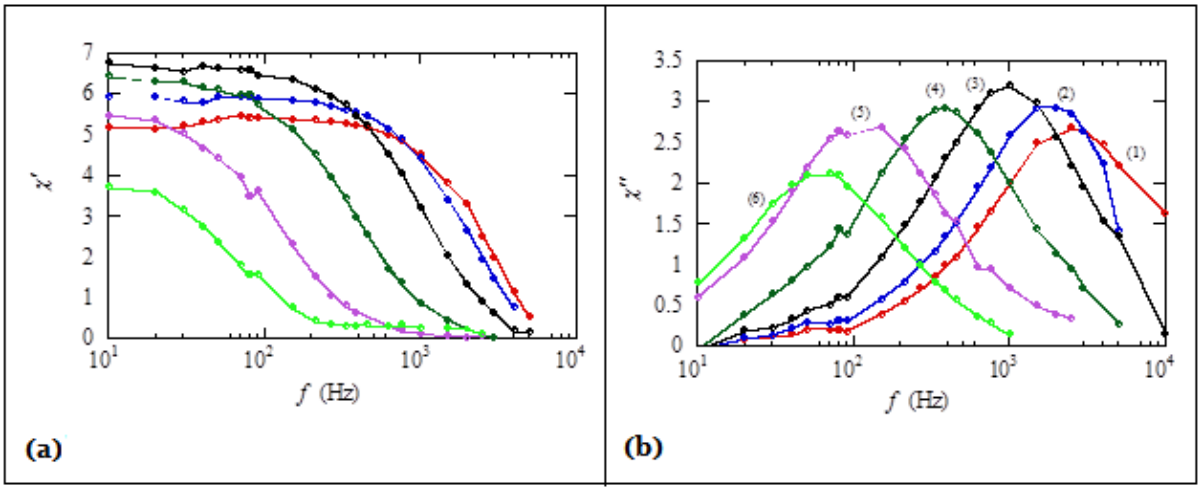

Fig. 2. Frequency dependence of the AC susceptibility for 6 samples listed in Table 1. (a) Real part χ', and (b) imaginary part χ".

Basic Theory of MNP and Particle Size Measurement

Numerical model used to measure particle size distribution

The nanoscale thermal motion and surface energy of MNPs, and their interaction with magnetic fields, obey the universal rules of statistical physics. The magnetization curve is obtained as a result of the combined action of magnetic fields and thermal motion. For a multi-size distribution system of *noninteracting* particles, the average magnetization is [13, 14, 15, 20].

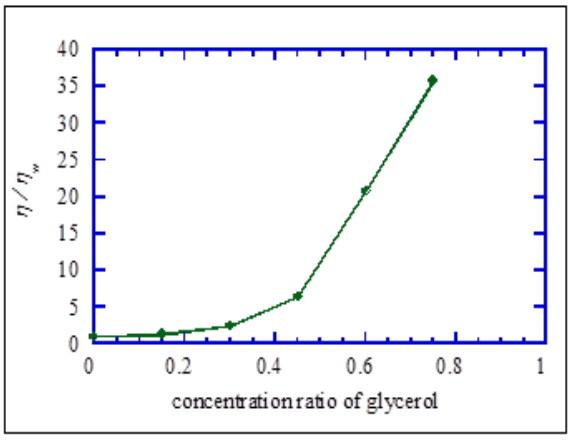

Fig. 3. Viscosity of the water/glycerol mixed solution as a function of glycerol concentration.

$$M(H) = \int \mu_0 M_d \, L(D,H) \frac{\pi D^3}{6} f(D)\, dD \qquad (3)$$

with $L(D,H) = L(\xi) = coth\xi - \frac{1}{\xi}$ (4)

$$\xi = \frac{\mu_0 M_d \frac{\pi}{6} D^3 H}{k_B T} \qquad (5)$$

where L denotes the Langevin function, D denotes the MNP diameter, f is the particle size distribution function, M_d is the saturation magnetization and H is the strength of the external magnetizing field. Magnetic moment information can be obtained using SQUID, VSM, or atomic force microscopy.

If the particle diameter D and magnetic field H_i are both given discrete values, the magnetization equation then becomes [14, 15],

$$M(H_i) = \sum_{j=1}^{N} \mu_0 M_d \frac{\pi}{6} D_j^3 L\left(\frac{\mu_0 M_d \frac{\pi}{6} D_j^3 H_i}{k_B T}\right) f(D_j) \Delta D_j \quad , i = 1, \ldots Z \qquad (6)$$

where N denotes the number of sampling points used for the particle diameter and Z represents the sampling steps used for the magnetizing field H_i. Thus, the magnetic moment matrix M can be rewritten as,

$$M(H_i) = A(i,j) f(D_j) \text{ or } M(i) = A(i,j) f(j) \text{ with}$$

$$A(i,j) = \mu_0 M_d \frac{\pi}{6} D_j^3 L\left(\frac{\mu_0 M_d \frac{\pi}{6} D_j^3 H_i}{k_B T}\right) \Delta D_j \quad , i = 1 \ldots Z, \; j = 1 \ldots N \qquad (7)$$

The magnetic properties of the MNPs can be described using a numerical matrix equation of the following form

$$M(i) = A(i, j) f(j) \qquad (8)$$

where $A(i, j)$ may be determined directly by the

magnetic physics of the MNP magnetization, $M(i)$ represents the magnetic curve and f (j) is the particle size distribution function. Details of this discretization and its effects on the ill-condition of the matrix equation, as well as a discussion of the range of particle sizes and magnetization fields used in the analysis.

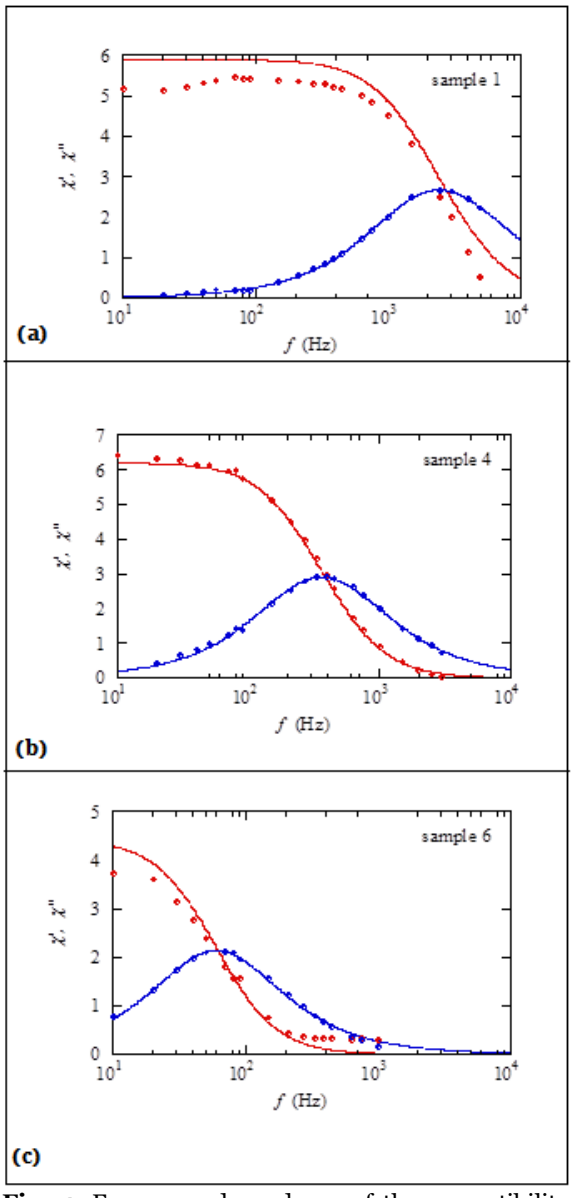

Fig. 4. Frequency dependence of the susceptibility. (a) sample 1, (b) sample 4, and (c) sample 6. The solid lines are calculated from Eqs. (1) and (2) by using the size distribution shown in Figure 5 the symbols are experimental results.

All the terms in equation (6) are non-negative. Because the particle size distribution function f (j) is the only unknown term, the estimation of particle size distribution may be reduced to the solution of a non-negative matrix equation.

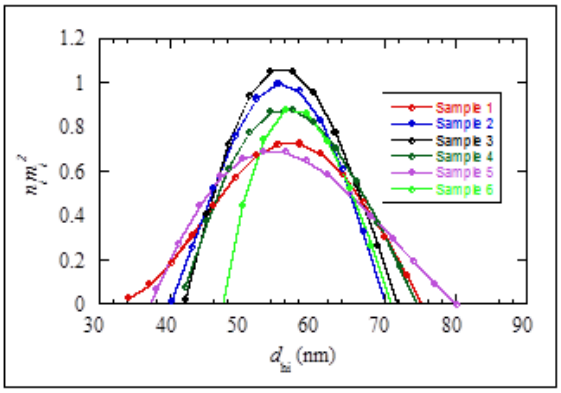

Fig. 5. Size distribution for the different mixed solution with water and glycerol.

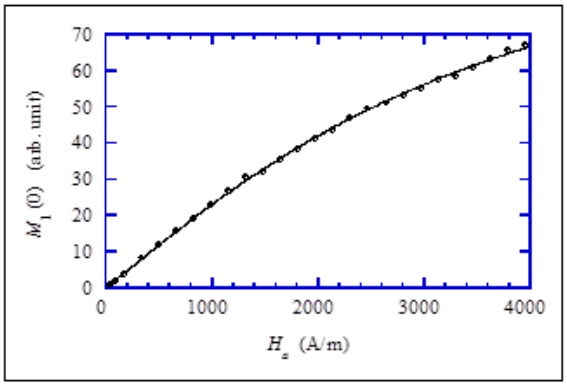

Fig. 6. Dependence of $M_1(0)$ on H_a. Circles represent the experimental results, while solid line represents the result calculated from eq. (9) using the estimated magnetic moment distribution shown in Figure 7. Eqs. (3)– (8) shows that the size distribution of a super-paramagnetic MNP system, whose magnetization is described by the Langevin equation, may be estimated using the methods presented herein, regardless of whether a water based or oil-based MNP is used. This model is the Numerical model used to measure particle size distribution.

In the study described herein, we obtained the detail method used to estimate the size distribution of the MNPs from the frequency dependence of AC susceptibility by SVD method [19, 20].

M-H Curve

In our experiment, we measured the magnetization of the markers in solution. In Figure. 6, the circles show the experimental results. Here, vertical axis

represents the value of magnetization M_1 at f = 0 Hz, $M_1(0)$, while the horizontal axis represents the amplitude H_a of the excitation field. In the experiment, the value of $M_1(0)$ was obtained from the value of $M_1(90\ Hz)$ since M_1 became constant independent of the frequency at low frequencies.

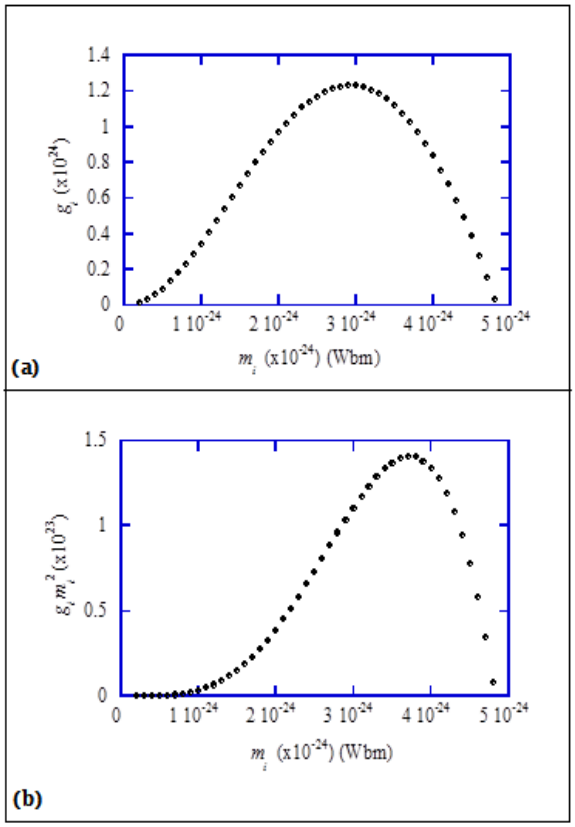

Fig. 7. Estimated distribution of magnetic moment of the markers. (a) g_i–m_i curve and (b) $g_i m_i^2$-m_i curve.

As shown, M_1 increased linearly at small values of H_a, while it began to saturate at higher H_a. It is known that this saturation of M was caused by the nonlinear effect of Brownian relaxation in high excitation fields. Expression for the M_1-H curve is given by [14, 15]

$$M_1(0)=\frac{H}{3\mu_0 k_B T V_T}\sum_i g_i(m_i)m_i^2\left[\frac{\chi_i(0)}{\chi_0}\right]\Delta m_i \approx \frac{H}{3\mu_0 k_B T V_T}\sum_i g_i m_i^2\left(1-\frac{\xi_i^2}{10+9\xi_i+3.81\xi_i^2+\xi_i^3}\right)\Delta m_i \quad (9)$$

where $g_i(m_i)$ is the distribution function of m, and

$$\xi_i = m_i H / k_B T \quad (10)$$

is the parameter representing the strength of the applied field. The relationship between the distribution function $f(d_h)$ and $g(m)$ is given as follows. Note that $g_i \Delta m_i$ is the number of particles with the magnetic momentm_i, while $f_i \Delta d_{hi}$ is the number of particles with diameter d_{hi}. Since these values should be the same, we obtain

$$f(d)\Delta d = g(m)\Delta m \quad (11)$$

Singular Value Decomposition Method (SVD)

SVD has been used to detect and characterize structural intermediates in biomolecular small-angle scattering experiments (Chen *et al.*, 1996). This study provides a good illustration of how SVD can be used to extract biologically meaningful signals from the data. Small-angle scattering data were obtained from partially unfolded solutions of lysozyme, each consisting of a different mix of folded, collapsed and unfolded states. The data for each sample was in the form of intensity values sampled at on the order of 100 different scattering angles. UV spectroscopy was used to determine the relative amounts of folded, collapsed and unfolded lysozyme in each sample. SVD was used in combination with the spectroscopic data to extract a scattering curve for the collapsed state of the lysozyme, a structural intermediate that was not observed in isolation.

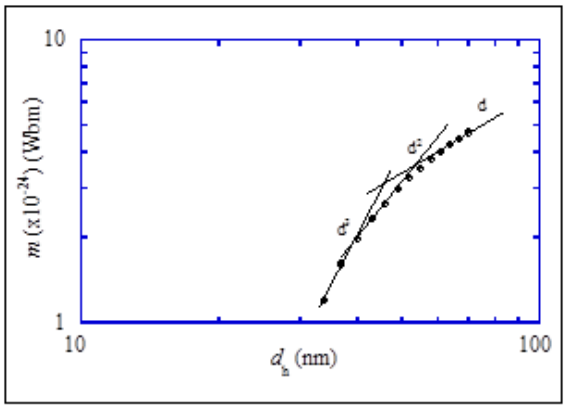

Fig. 8. Estimated size dependences of magnetic moment m. The results were obtained by combining the $n_i m_i^2$-d_{hi} curve shown in Figure. 5 and the $g_i m_i^2$-m_i curve shown in Figure 7 (b).

In this work, we apply the SVD method for the calculation of size distribution of the practical marker. Since the frequency dependence of the susceptibility is theoretically given by Eqs. (1) and (2), we can estimate the size distribution of the markers by comparing the experimental results with the

theoretical ones, as shown below. In the comparison, we first choose N sets of τ_i $(i = 1,\ldots,N)$ in Eqs. (1) and (2).

Then we take $n_i m_i^2$ as unknown values, and determine the values of $n_i m_i^2$ so as to obtain the best fit between the experimental and theoretical results. With this technique we can obtain the $\tau_i - n_i m_i^2$ curve. This curve is transformed in to the $d_{hi} - n_i m_i^2$ curve using Eq. (1), which gives the size distribution of the markers.

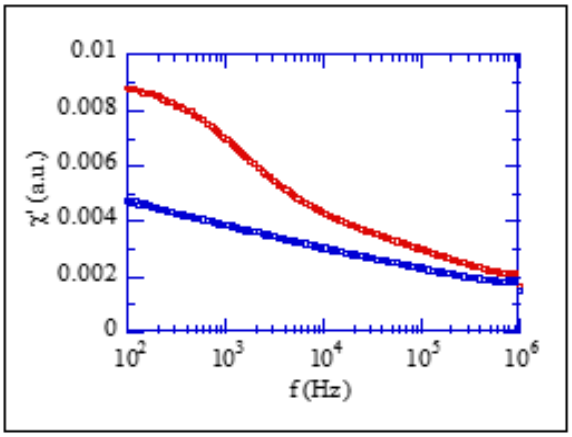

Fig. 9. Frequency dependence of real part of the AC susceptibility. χ'_{sus} and χ'_{imm} represents the real part of the susceptibilities in suspension and immobilized cases, respectively.

To determine the values of $n_i m_i^2$ in the presence of experimental error in the practical data, we use the mathematical technique known as SVD method. Details of the SVD methods are described in refs [16, 17].

Magnetic moment

Distribution of Magnetic Moment m

Next, we estimate the distribution of magnetic moment m from the magnetization curve shown in Figure 6. For this purpose, we compare the experimental results with Eq. (9). In this case, we first choose N sets of m_i (i = 1,... N) in Eq. (9). Then we take g_i as unknown values, and determine the values so as to obtain the best fit between the experimental and theoretical results by using the SVD method.

In Figure 7 (a), the estimated distribution of m, i.e., g_i-m_i curve is shown. As shown, the value of m distributed from 5×10^{-25} to 5×10^{-24} Wbm with mean value of m=3×10^{-24} Wbm. For the following discussion, we also show in Figure 7 (b) the $g_i m_i^2$-m_i curve. Substituting the distribution of m shown in Figure 7 (a) into Eq. (9), we could reconstruct the *M-H* curve. In Figure 6, the solid line shows the reconstructed results. As shown, good agreement was obtained between the experimental and reconstructed results. This agreement indicates the validity of the estimation of m distribution.

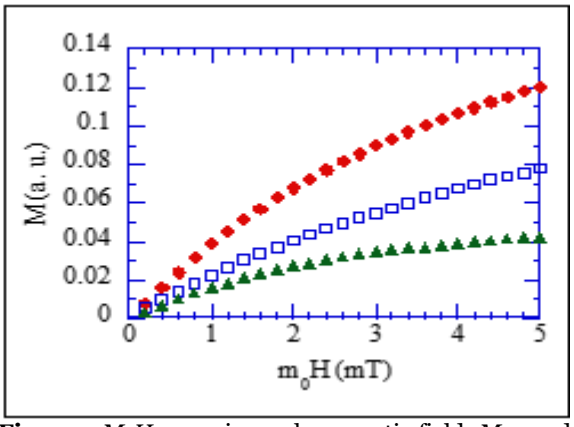

Fig. 10. *M-H* curve in weak magnetic field. M_{sus} and M_{imm} represent the magnetizations in suspension and immobilized cases, respectively.

Relationship between m and d

We now discuss the relationship between the magnetic moment m and size d. In the case of single domain particles, it is well known that m is proportional to the volume of the particle, i.e., m is proportional to d^3.

In practical markers, however, aggregation of particles occurs in making markers. Therefore, it is expected that the magnetic marker consisted of agglomerate of particles. In this case, the magnetic moments of individual particles within the agglomerate should not align in the same direction, i.e., agglomerate of particles will behave like multi-domain particles. As a result, simple relationship that m is proportional to d^3 should be modified in this case.

The relationship between m and d can be obtained by combining the $n_i m_i^2$-d_{hi} curve shown in Figure 5 and the $g_i m_i^2$-m_i curve shown in Figure 7 (b). In Figure 8,

circles represent the estimated dependence of m on d. As shown, m increased in proportion to the d^3 for the case of d<40 nm. This relationship is consistent with the result of single domain particles. When d becomes larger, on the other hand, dependence of m on d changed: m becomes proportional to d^2, and then proportional to d with the increase of d. It must be noted that Fe_3O_4 is expected to form the single domain particle when the diameter d is less than 40 nm, while it forms the multi-domain particle for the case of d >40 nm. The result shown in Figure 8 is consistent with this prediction.

We have also measured the frequency dependence of the real part of the AC susceptibility (χ') and magnetization (M-H) curves of different commercial markers. Examples are shown in Figure. 9 and Figure. 10, where both results for suspension and immobilized samples are shown. Analyzing these data, we can obtain the parameters of the markers, such as hydrodynamic diameter d_h, magnetic moment m, and anisotropy energy E_B [22]. In Type-I markers, magnetic interaction is negligible, and hence they have small values of m and E_B (or short Neel relaxation time τ_N). In Type-II markers, magnetic interaction is medium, and hence they have large m and medium E_B (or medium τ_N). In Type-III markers, magnetic interaction is strong, and hence they have large m and E_B (or long τ_N). As shown in Figure 9, we can estimate the contribution of each type of markers to the susceptibility signal. Type III markers give the difference in the susceptibility between the suspension (χ'_{sus}) and immobilized (χ'_{imm}) cases. Contribution of Type II and Type I markers can be estimated by the susceptibility in low and high frequency region of the immobilized sample, respectively. Similarly, in Figure 10, type III markers give the difference in the magnetization between the suspension (M_{sus}) and immobilized (M_{imm}) cases. Nonlinearity of M-H curve of the immobilized case in weak field is dominated by the Type II markers. Since Type-III makers contribute to the signal in liquid-phase immunoassays using Brownian relaxation, it is important to choose a sample having a large portion of Type-III markers.

Conclusions

We have characterized the magnetic properties of magnetic markers in solution for biosensor application. Frequency dependence of the AC susceptibility and the magnetization curve, which were dominated by the Brownian rotation of the marker, were measured. The effect of the viscosity of the carrier liquid on the AC susceptibility was also clarified. The experimental results were analyzed by the singular value decomposition (SVD) method.

The distribution of marker size d was obtained from the frequency dependence of the susceptibility. The distribution of magnetic moment m was obtained from the magnetization curve. The relationship between m and d was also discussed. The present estimation method using SVD technique will be useful to obtain the distribution of d and m, which are the important parameters of the magnetic marker for biosensor application.

Acknowledgement

This research work has been done with the financial support of MEXT, JAPAN under RISS Lab Kyushu University, Fukuoka, Japan.

The researchers also acknowledge the supports of Bangladesh Atomic Energy Commission and Superconductor Lab, Department of Physics and Information Technology, Faculty of Computer Science and Systems Engineering, Kyushu Institute of Technology, Iizuka, Fukuoka, 820-8502 Japan.

Declaration

All the authors do not have any possible conflicts of interest.

References

1. J. Phys. D: Appl. Phys. **36** (2003) R167–R181.
2. Handbook of Magnetic Nanoparticles. Sergey P. Gubin.
3. Q. A. Pankhurst, N. K. T. Thanh, S. K. Jones, and J. Dobson: J. Phys. D: Appl. Phys. **42** (2009) 224001.

4. C. C. Berry: J. Phys. D: Appl. Phys. **42** (2009) 224003.
5. M. Lu, F. Ibraimi, D. Kriz, and K. Kriz: Biosens. Bioelectron. **21** (2006) 2248.
6. M. J. Chiu, H. E. Horng, J. J. Chien, S. H. Liao, C. H. Chen, B. Y. Shih, C. C. Yang, C. L. Lee, T. F. Chen, S. Y. Yang, C. Y. Hong, and H. C. Yang: IEEE Trans. Appl. Supercond. **21** (2011) 477.
7. H. Grossman, W. Myers, V. Vreeland, R. Bruehl, M. D. Alper, C. R. Bertozzi, and J. Clarke: PNAS U.S.A. **101** (2003) 129.
8. L. Néel, C. R. Hebd. Seances Acad. Sci. **228**, 664 (1949); Ann. Géophys. **5**, 99 (1949).
9. W. F. Brown, Phys. Rev. **130**, 1677 (1963).
10. Eberbeck D, Bergemann C, Hartwig S, Steinhoff U and Trahms L 2005 Binding kinetics of magnetic nanoparticles on latex beads and yeast cells studied by magnetorelaxometry *J. Magn. Magn. Mater.* **289** 435–8.
11. Enpuku K, Kuroda D, Ohba A, Yang T Q, Yoshinaga K, Nakahara T, Kuma H and Hamasaki N 2003 Biological immunoassay utilizing magnetic marker and high *Tc* superconducting quantum interference device magnetometer *Japan. J. Appl. Phys.* **42** L1436–8.
12. Ludwig F, Maeselein S, Heim E and Schilling M 2005 Magnetorelaxometry of magnetic nanoparticles in Meas. Sci. Technol. **20** (2009) 125802 WLiu *et al* magnetically unshielded environment utilizing a differential fluxgate arrangement *Rev. Sci. Instrum.* **76** 106102.
13. Rosensweig R E 1985 *Ferrohydrodynamic* (Cambridge: Cambridge University Press).
14. Romanus E, Berkov D V, Prass S, Gross C, Weitschies W and Weber P 2003 Determination of energy barrier distributions of magnetic nanoparticles by temperature dependent magnetorelaxometry *Nanotechnology* **14** 1251–4.
15. K. Enpuku, T. Tanaka, M. Matsuda, F. Dang, N. Enomoto, J. Hojo, K. Yoshinaga, F. Ludwig, F. Ghaffari, E. Heim, and M. Schilling: J. Appl. Phys. 102 (2007) 054901.
16. Brown W F Jr 1963 Thermal fluctuations of a single-domain particle *Phys. Rev.* **130** 1677–86.
17. Yuichi Higuchi, Shinobu Uchida, ***Anwarul Kabir Bhuiya***, Takashi Yoshida, and Keiji Enpuku, "Characterization of Magnetic Markers for Liquid-Phase Detection of Biological Targets" IEEE TRANSACTIONS ON MAGNETICS, VOL. 49,); NO. 7, July 2013.
18. ***Anwarul Kabir Bhuiya***, Masaki Asai, Hideki Watanabe, Tomokazu Hirata, Yuichi Higuchi, Takashi Yoshida, and Keiji Enpuku, "Characterization of Magnetic Markers and Sensors for Liquid-Phase Immunoassays Using Brownian Relaxation". IEEE TRANSACTIONS ON MAGNETICS, VOL. 48,) p2838-2841; NO. 11, NOVEMBER
19. ***Anwarul Kabir Bhuiya***, Tetsu Mitake, Masaki Asai, Tomoya Ito, Schunichi Chosakabe, Takashi Yoshida, Keiji Enpuku, and Akihiko Kandori, "Liquid-Phase Immunoassays Using Brownian Relaxation of Magnetic Markers". IEEE TRANSACTIONS ON MAGNETICS, VOL. 47,) p2867-2870; NO. 10, OCTOBER 2011.
20. ***Bhuiya, Anwarul Kabir*;** Yoshida, Takeshi; Enpuku, Keiji, "Characterization of Magnetic Markers for Bio-sensing Application". Research reports on information science and electrical engineering of Kyushu University 15(2) p77-83; 2010-09-24.

21. ***Anwarul Kabir BHUIYA***, Masaki ASAI, Takashi YOSHIDA and Keiji ENPUKU, "Magnetic Sensor Based Liquid-Phase Immunoassays for the Detection of Biological Targets". Research reports on information science and electrical engineering of Kyushu University 16(2) p45-50; 2011-09-26.

22. K. Enpuku et al., "Characterization of Magnetic Markers for Liquid-Phase Immunoassays Using Brownian Relaxation", Jpn. J. Appl. Phys., 51, 023002, 2012.